CO_2 Sorption on MgO and CaO Surfaces: A Comparative Quantum Chemical Cluster Study

Morten B. Jensen,[†] Lars G. M. Pettersson,[‡] Ole Swang,*[,§] and Unni Olsbye*[,†]

Center for Materials Science and Nanotechnology, Department of Chemistry, University of Oslo, P.O. Box 1033 Blindern, N-0315 Oslo, Norway, FYSIKUM, AlbaNova, Stockholm University, S-10691 Stockholm, Sweden, and Department of Hydrocarbon Process Chemistry, SINTEF Materials and Chemistry, P.O. Box 124 Blindern, N-0314 Oslo, Norway

Received: April 20, 2005; In Final Form: June 18, 2005

A comparative quantum chemical study of CO_2 adsorption on MgO and CaO has been carried out. Theoretical infrared (IR) frequencies are calculated and compared with IR experiments from the literature. The results show that CO_2 adsorbs as monodentate on edge sites and bidentate on corner sites on MgO. The former assignment contradicts the common assumption of adsorption of CO_2 in a bidentate configuration. On CaO, CO_2 adsorbs as monodentate on both edge and corner sites, which is a reinterpretation of earlier experimental work. On terrace (100) sites, none of the adsorption modes on MgO or CaO possess calculated frequencies in agreement with the experimental IR spectra. These experimental bands were tentatively assigned to some slightly perturbed double negatively charged carbonate ions at the surface, rather than the monodentate structure suggested in the literature.

1. Introduction

Basic oxides, especially MgO, are known as suitable catalyst support materials for a number of reactions, such as alkane conversion reactions.[1−6] Recently, MgO- and CaO-like materials have received increased attention as adsorbents for CO_2, in particular for hydrogen production from methane:[7−11] Methane is converted to synthesis gas ($CO + H_2$) by wet or dry reforming; see eqs 1 and 2. The associated water gas shift

$$CH_4 + H_2O = CO + 3\,H_2 \quad (1)$$

$$CH_4 + CO_2 = 2CO + 2\,H_2 \quad (2)$$

$$CO + H_2O = H_2 + CO_2 \quad (3)$$

$$CO_2 + M{-}O(s) = M{-}O{-}CO_2(s) \quad (4)$$

$$CH_4 + 2H_2O = 4H_2 + M{-}O{-}CO_2(s) \quad (5)$$

reaction (eq 3) may be altered by CO_2 capture (eq 4), leading to hydrogen as the only gaseous reaction product (eq 5). While hydrogen may be stored or used directly as a nonpolluting fuel, CO_2 may be isolated and transported to a storage site.

It has recently been proposed that MgO is not only a potential CO_2 adsorbent but may also play an active role in the catalytic dry reforming of methane to synthesis gas (2) over supported metal catalysts:[12] $Mg{-}O{-}CO_2$ is proposed to interact with the metal surface, thereby facilitating oxidation of CH_x species to CO (and water), and significantly reducing coke production. Such an active role of MgO has, however, been disputed.[13]

Fukuda and Tanabe[14] studied CO_2 adsorption on MgO and CaO powders by infrared (IR) spectroscopy. After CO_2 adsorption at room temperature, they observed bands that were assigned to uni- and bidentate carbonate on MgO. The fraction of "bidentate" carbonate decreased with increasing loading, but increased with increasing outgassing temperature. On CaO, the only observed bands at room temperature were assigned to unidentate carbonate. At 350 °C, bands that were assigned to bidentate carbonate were observed also for CaO. Yanagisawa et al.[15] performed temperature-programmed desorption (TPD) and IR studies of CO_2 and ^{18}O-enriched CO_2 on MgO powder. They found two distinct carbonate groups on MgO: The least stable carbonate group was assigned to a monodentate species by means of ab initio molecular modeling studies.[16] $C^{18}O_2$ adsorption experiments showed that single and double oxygen exchange with the $Mg^{16}O$ lattice took place, yielding $C^{18}O^{16}O$ and $C^{16}O_2$, respectively. From TPD measurements, the activation energy of desorption, E_d, for the double oxygen exchange CO_2 was estimated to ∼1.2 eV (116 kJ/mol).[16] Ab initio molecular modeling calculations indicated that oxygen exchange takes place after bidentate adsorption at a three-coordinated O^{2-} corner site.[16] Dumesic et al.[17] performed calorimetric measurements of CO_2 adsorption on MgO and reported adsorption enthalpies ranging from 80 to 170 kJ/mol depending on coverage. Recently, Carrier et al.[18] performed synchrotron-based photoemission spectroscopy and NEXAFS spectroscopy of CO_2 adsorption on a MgO (100) crystal and found formation of carbonate as well as a different form of carbon.

To elucidate the potential role of MgO and CaO as adsorbents and catalytic sites in CO_2 conversion reactions, detailed knowledge about the $M{-}O{-}CO_2$ interaction is required. The present work is devoted to theoretical modeling of $M{-}O{-}CO_2$ interactions (M = Mg, Ca). Some results of this kind have already been published: Pacchioni[19] performed ab initio SCF calculations and concluded that CO_2 physisorbs, linearly end-on or horizontally oriented, onto MgO terraces. At four-

* To whom correspondence should be addressed. E-mail: unni.olsbye@kjemi.uio.no; ole.swang@sintef.no.
[†] University of Oslo.
[‡] Stockholm University.
[§] SINTEF Materials and Chemistry.

10.1021/jp052037h CCC: $30.25
Published on Web 08/12/2005

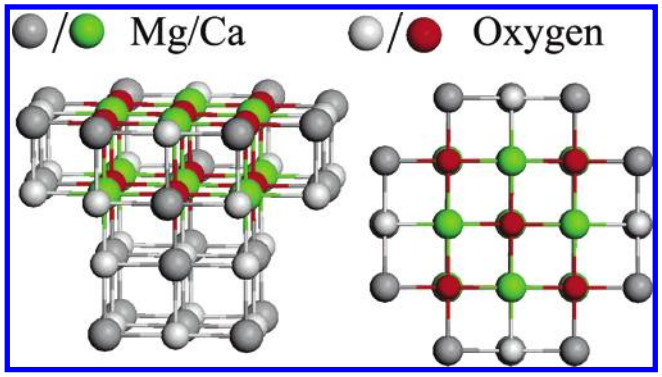

Figure 1. Cluster model of MgO/CaO terrace site, front (left) and top (right) view. Gray atoms are treated with the 6-31G basis set and colored with the 6-31G(d) basis set. Only the colored surface atoms were relaxed during geometry optimizations.

coordinated step sites, carbonate formation was found to take place. Comparative studies[20−23] of CO_2 (and SO_2) adsorption on MgO and CaO (100) surfaces, using ab initio cluster model calculations, indicated that CO_2 adsorbs weakly on MgO (in accordance with the above), while carbonate species are formed on CaO. Recently, Karlsen et al.[24] studied the interaction between NO_x, SO_x, and CO_2 with M−O (001) terrace sites (M = Mg, Ca, Sr, Ba) by using an embedded cluster model. They found that CO_2 is horizontally physisorbed on the MgO terrace sites, while chemisorption, accompanied by significant distortion of the C−O bond lengths and angles, is observed on CaO. Cluster models of MgO have been widely used to study adsorption of small molecules (most notably CO) on the oxide surface. The number of published investigations employing CaO cluster models is more limited, but some publications have appeared.[20,24−26] It is by now generally accepted that cluster models, as employed in the present study, may offer a useful description of local surface properties of alkaline-earth oxides.[25,27−29] More specifically, it has been thoroughly demonstrated that a bare cluster model works very well for CO sorption on MgO.[30,31]

In the present work, we will compare CO_2 adsorption at regular (terrace) and defect (step and corner) sites on the (100) face of both MgO and CaO. We will focus on the predicted vibrational frequencies in an effort to provide a strong interpretation of the available experimental data.

2. Computational Details

The CO_2 interaction with O^{2-} sites on MgO and CaO surfaces has been investigated by means of a cluster model approach. Various adsorption sites have been considered: five-coordinated O^{2-} on regular (100) surfaces (O_{5C}), four-coordinated O^{2-} at edges (O_{4C}), and three-coordinated O^{2-} at corners (O_{3C}). The stoichiometric MO (M = Ca/Mg, O = oxygen) clusters used are $M_{30}O_{30}$ for terrace, $M_{24}O_{24}$ for edges, and $M_{19}O_{19}$ for corners; see Figures 1−3. The lattice constants used to construct the MgO and CaO clusters are respectively 4.21 and 4.81 Å.

Density functional theory (DFT) calculations were performed using the B3LYP hybrid density functional as implemented in the Gaussian 03 package.[32] The 6-311+G(d) basis set was used for the CO_2 molecule and a combined 6-31G/6-31G(d) basis set for the metal oxides, where the 6-31G(d) basis set was used for atoms near the adsorption site. Some test calculations were carried out with a number of larger basis sets on a very small cluster to investigate basis set convergence; see below. Partial geometry optimizations were carried out allowing the CO_2 molecule and the surface atoms described by the 6-31G(d) basis set to relax freely, while the other atoms were kept fixed at bulk values. The geometry optimizations were kept constrained to C_{2v} symmetry for CO_2 on O_{5C} and O_{4C} and to C_s for CO_2 on O_{3C}. Calculations of IR spectra show no imaginary frequencies, confirming that the energy minimums in question indeed have these symmetries.

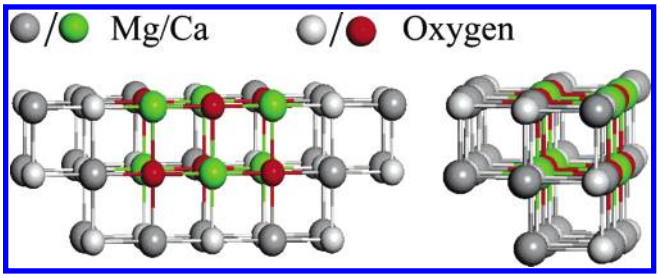

Figure 2. Cluster model of MgO/CaO edge site, front (left) and side (right) view. Gray atoms are treated with the 6-31G basis set and colored with the 6-31G(d) basis set. Only the colored surface atoms were relaxed during geometry optimizations.

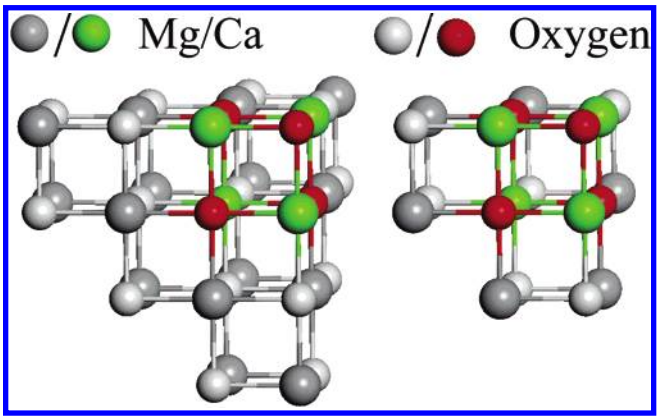

Figure 3. Cluster models of MgO/CaO corner site. Gray atoms are treated with the 6-31G basis set and colored with the 6-31G(d) basis set. Only the colored surface atoms were relaxed during geometry optimizations. The reduced model (right) was employed to estimate the BSSE energies due to SCF convergence problem; see computational section.

The DFT adsorption energies have been corrected for the basis set superposition error (BSSE) by applying the standard counterpoise method as implemented in Gaussian 03.[33] The counterpoise calculations do not include geometry optimizations; hence, they are purely single-point corrections to the energies. Due to SCF convergence problems for CO_2 at corner sites, clusters of reduced size (M_9O_9) have been used to estimate the BSSE energies for the O_{3c} site; see Figure 3 for the cluster employed. Test calculations showed that BSSE energies were fairly independent of the cluster size. The DFT adsorption energy is defined as

$$E_{ads} = (E_{MO/CO_2} + E_{BSSE}) - (E_{MO} + E_{CO_2})$$

where E_{MO/CO_2} is the energy of the CO_2/MO cluster, E_{BSSE} is the basis set superposition error energy, E_{MO} is the energy of the bare MO cluster, and E_{CO_2} is the energy of the isolated CO_2 molecule.

Harmonic vibrational frequencies of CO_2 at low-coordinated O^{2-} adsorption sites have been computed by determining the analytical second derivatives of the total energy with respect to the internal coordinates. No empirical scaling factors were applied to the computed frequencies. Throughout, negative sorption energies indicate that the sorption is exothermal.

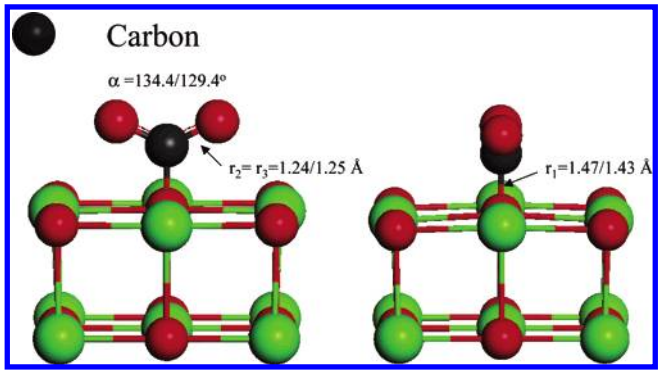

Figure 4. Monodentate adsorption at MgO/CaO terrace site. The $[O_s-CO_2]^{2-}$ unit is coplanar with the two adjacent surface Mg^{2+}/Ca^{2+} ions. Numbers before and after the slash represent bond distances or angles for CO_2 on MgO and CaO, respectively. Reduced clusters depicted for clarity.

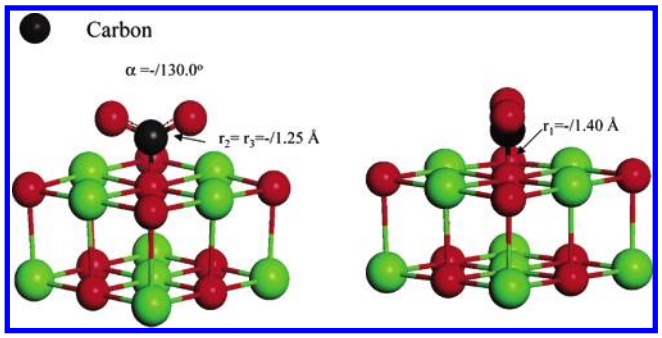

Figure 5. Monodentate adsorption at CaO terrace site. No local energy minimum was found for this orientation on MgO. The $[O_s-CO_2]^{2-}$ unit forms a dihedral angle of 45° with the surface Ca^{2+} ions. Reduced clusters depicted for clarity.

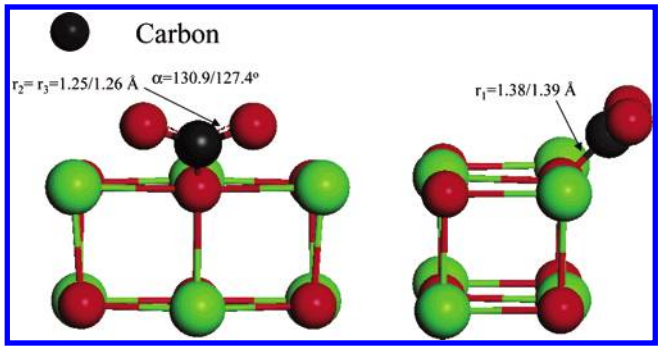

Figure 6. Monodentate adsorption at MgO/CaO edge site. Numbers before and after the slash represent bond distances or angles for CO_2 on MgO and CaO, respectively. Reduced clusters depicted for clarity.

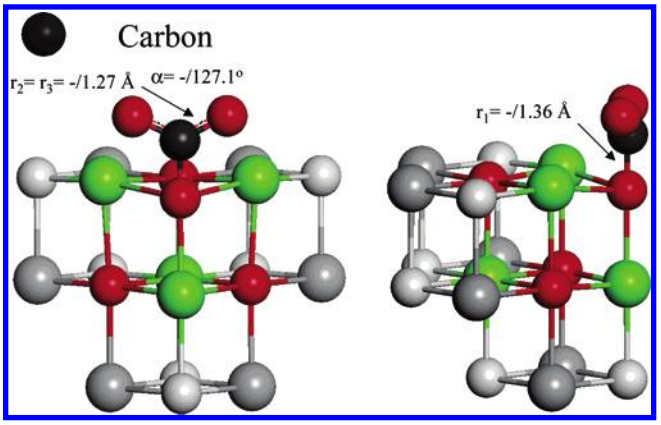

Figure 7. Monodentate adsorption at CaO corner site (an energetically stable monodentate sorption mode on MgO was not found). Reduced clusters depicted for clarity.

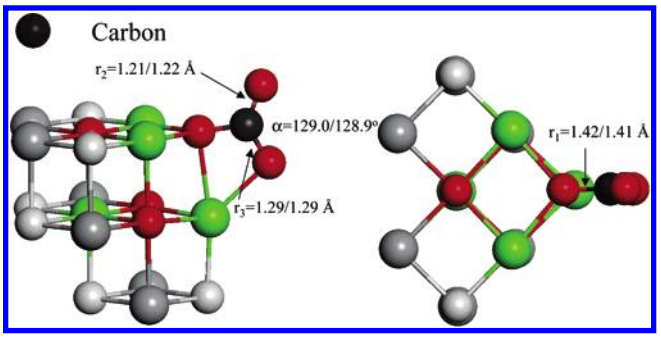

Figure 8. Bidentate adsorption at MgO/CaO edge site. Numbers before and after the slash represent bond distances or angles for CO_2 on MgO and CaO, respectively. Reduced clusters depicted for clarity.

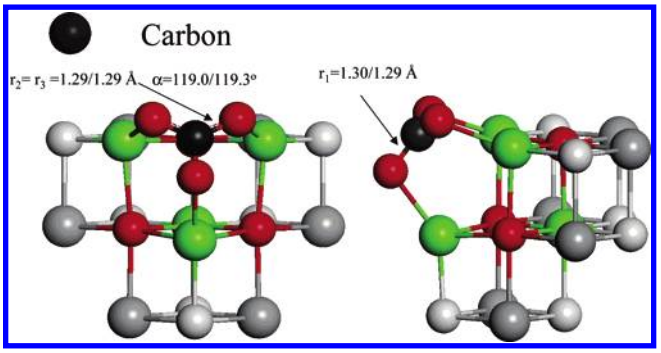

Figure 9. Tridentate adsorption at MgO/CaO edge site. Numbers before and after the slash represent bond distances or angles for CO_2 on MgO and CaO, respectively. Reduced clusters depicted for clarity.

3. Results and Discussion

When CO_2 interacts with a basic metal oxide surface, a charge transfer from a surface anion, O^{2-}, to the CO_2 molecule may lead to energetically favorable surface carbonate species. Since the interaction is assumed to mainly be of HOMO−LUMO type,[19] the nature of the formed carbonate species depends on the coordination number of the surface oxygen. The LUMO of CO_2 is highest in energy of the two interacting frontier orbitals, but the HOMO energy level of surface oxygen increases with decreasing coordination number. Consequently, the HOMO−LUMO energy gap between O^{2-} and CO_2 is reduced on defect sites and thus charge transfer from O^{2-} to CO_2 will occur at lower energy cost for O_{3c} and O_{4c} sites compared with regular O_{5c} sites. Various geometry optimized adsorption structures of CO_2 on MgO and CaO are shown in Figures 4−9. Adsorption of CO_2 on O_{5C} is depicted in Figures 4 and 5, on O_{4C} in Figure 6, and on O_{3C} in Figures 7−9. The configurations shown in Figures 4−7 are so-called monodentates, in Figure 8 bidentate, and in Figure 9 tridentate. Theoretical IR spectra of the above-mentioned configurations are compared with experimental IR spectra from the literature in an attempt to assign the latter and to decide the actual structure of the species sorbed on the surface.

The gaseous carbonate ion may form a basis for understanding the frequencies arising from the carbonate-like species on the surface. The free carbonate ion has one Raman-active mode at 1063 cm^{-1}(ν_1; symmetric CO stretch), one IR-active mode at 879 cm^{-1} (ν_2; out-of-plane deformation), and one doubly degenerate, IR-active mode at 1415 cm^{-1} (ν_3; asymmetric CO stretch).[34] Loss of symmetry results in infrared activation of the ν_1 and splitting of ν_3; the ν_3 splits into ν_{3h} and ν_{3l} (h = high, l = low frequency). Our calculated frequencies and DFT adsorption energies for different sorbed species are shown in

TABLE 1: Calculated Wavenumbers, IR Intensities, and Adsorption Energies of CO_2 at Various MgO Sites[a]

ads mode	ν_{3h} (cm^{-1})	ν_{3l} (cm^{-1})	ν_1 (cm^{-1})	ν_2 (cm^{-1})	E_{ads} (kJ/mol)
terrace,[b] O_{5c}, dih ang 0°	1784 (391)	1288 (164)	827 (209)	821 (13)	13
terrace,[c] O_{5c}, dih ang 45°					
step, O_{4c}	1703 (658)	1327 (354)	1011 (198)	849 (21)	−154
corner,[d] O_{3c}, monodentate					
corner, O_{3c}, bidentate	1778 (867)	1243 (211)	932 (403)	847 (20)	−115
corner, O_{3c}, tridentate	1451 (279)	1451 (285)	1084 (23)	906 (40)	−152

[a] IR intensities (KM/mol) are given in parentheses. [b] The $[O_s\text{-}CO_2]^{2-}$ unit is coplanar with the two adjacent surface Mg^{2+} ions. [c] The $[O_s\text{-}CO_2]^{2-}$ unit forms a dihedral angle of 45° with the surface Mg^{2+} ions. No local energy minimum was found for this orientation. [d] No energetically stable monodentate was found at the corner site.

TABLE 2: Calculated Wavenumbers, IR Intensities, and Adsorption Energies of CO_2 at Various CaO Sites[a]

ads mode	ν_{3h} (cm^{-1})	ν_{3l} (cm^{-1})	ν_1 (cm^{-1})	ν_2 (cm^{-1})	E_{ads} (kJ/mol)
terrace,[b] O_{5c}, dih ang 0°	1708 (340)	1298 (157)	876 (150)	847 (9)	−100
terrace,[c] O_{5c}, dih ang 45°	1692 (317)	1304 (157)	927 (117)	868 (13)	−60
step, O_{4c}	1664 (762)	1316 (424)	968 (227)	845 (13)	−219
corner, O_{3c}, monodentate	1603 (333)	1314 (425)	1035 (136)	876 (23)	−222
corner, O_{3c}, bidentate	1703 (737)	1257 (383)	944 (394)	845 (14)	−182
corner, O_{3c}, tridentate	1461 (302)	1423 (302)	1080 (11)	881 (43)	−164

[a] IR intensities (KM/mol) are given in parentheses. [b] The $[O_s{-}CO_2]^{2-}$ unit is coplanar with the two adjacent surface Ca^{2+} ions. [c] The $[O_s{-}CO_2]^{2-}$ unit forms a dihedral angle of 45° with the surface Ca^{2+} ions.

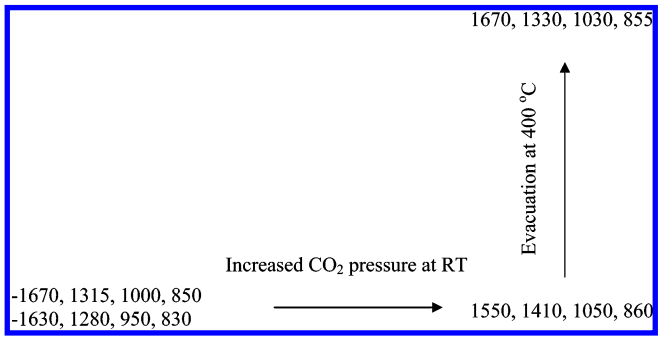

Figure 10. Schematic summary of infrared bands of CO_2 on MgO at various CO_2 concentration and evacuation temperatures reported by Fukada et al.[14]

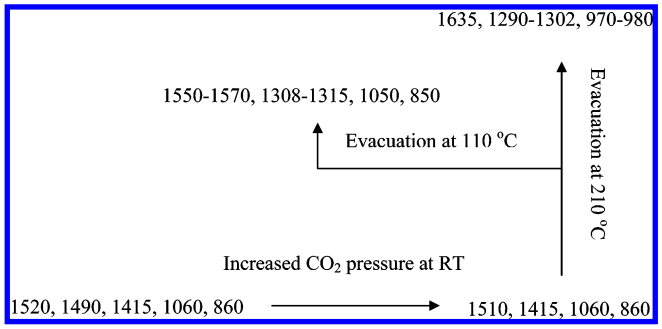

Figure 11. Schematic summary of infrared bands of CO_2 on CaO at various CO_2 concentration and evacuation temperatures reported by Fukada et al.[14]

Tables 1 and 2. As seen from these tables and from Figures 10 and 11, the ν_2 vibration is almost independent of the adsorption mode, and hence, it will not be discussed further.

Experimental infrared adsorption spectra of CO_2 on MgO and CaO are taken from Fukuda and Tanabe, where the surface areas measured by nitrogen adsorption were 158 and 52 m^2/g for MgO and CaO, respectively.[14] When MgO was exposed to CO_2 at low pressures and room temperature, they observed two distinct sets of bands at 1670, 1315, 1000, and 850 cm^{-1}, and 1630, 1280, 950, and 830 cm^{-1}. Increasing the pressure led to broad bands at 1550, 1410, 1050, and 860 cm^{-1}, while the intensities of the other bands decreased. Evacuation at 400 °C led to bands at 1670, 1330, 1030, and 855 cm^{-1}. In the case of CaO, bands at 1520, 1490, 1415, 1060, and 860 cm^{-1} were observed at room temperature. With an increase in the amount of CO_2, the intensities of the bands increased, and finally, the bands at 1520 and 1490 cm^{-1} merged into one band at 1510 cm^{-1}. Further, upon evacuation at temperatures between 110 and 210 °C, the bands at 1510, 1415, 1060, and 860 cm^{-1} disappeared, and new bands at 1635, 1290−1302, and 980 cm^{-1} and 1550−1570, 1308−1315, 1050, and 850 cm^{-1} appeared. The results are summarized in Figures 10 and 11.

3.1. Adsorption at Five-Coordinated O^{2-}. *MgO.* The DFT calculations suggest that CO_2 interaction with five-coordinated O^{2-} is not energetically favorable (Table 1), consistent with previously reported Hartree−Fock calculations.[19,20] Further, the calculated wavenumbers, 1784, 1288, 827, and 821 cm^{-1} are not comparable to any of the observed IR bands (Figure 10), and we may reasonably conclude that CO_2 adsorption on the unperturbed MgO(100) surface does not occur. Bending of the CO_2 molecule indicates some charge transfer from the MgO surface, but the O═C═O angle is larger than what is found for sorption at lower coordinated O^{2-}sites (see Figures 4−8). This result implies that charge transfer is less favorable on the regular (100) surface and does not occur to a sufficient degree to energetically stabilize the surface carbonate species.

CaO. The reactivity of CO_2 on CaO is very different from that on MgO, a fact that may be ascribed to the difference in the Madelung potential. The Madelung potential is ∼2.8 eV lower for CaO than MgO at O_{5C} sites,[35] due to the increased lattice constant. As a consequence, O^{2-} is less stabilized at the CaO surface. Lowering of the Madelung potential leads to a spatially more diffuse electron cloud of the O_{5C} site, which may overlap more efficiently with accepting orbitals of adsorbing molecules.[19,20,24] This is confirmed by the calculated adsorption energies for the two types of monodentates found on the terrace site, one where the $[O_s{-}CO_2]^{2-}$ unit is coplanar with the two adjacent surface Ca^{2+} ions (Figure 4) and another, less stable monodentate where the $[O_s{-}CO_2]^{2-}$ unit forms a dihedral angle of 45° with the surface Ca^{2+} ions (Figure 5). The calculated adsorption energies for the two orientations are −100 and −60 kJ/mol, respectively. The C−O bond distances and angles are nearly identical for the two species, but the former is probably electrostatically stabilized due to the shorter Ca^{2+}−OCO bond distance. Although the DFT adsorption energies are negative,

i.e., suggesting stable adsorption modes, the calculated frequencies for the two monodentates ($\nu_{3h} = 1708$, $\nu_{3l} = 1298$, $\nu_1 = 876$, and $\nu_{3h} = 1692$, $\nu_{3l} = 1304$, $\nu_1 = 927$) do not reproduce any of the wavenumbers of the experimentally observed carbonate-like species on CaO (Figure 11). In addition, the reported experimental adsorption enthalpy is in the range 140−200 kJ/mol, depending on coverage,[36,37] considerably higher than the DFT adsorption energies on terrace sites. Hence, the monodentate geometries found are probably not the preferred adsorption modes on the CaO (100) surface.

3.2. Adsorption at Four-Coordinated O^{2-}. *MgO*. In accordance with the expected reduction in the HOMO−LUMO energy gap compared with terrace sites, the monodentate formed at edges is more stable than on the terrace.[19,20] This is also reflected in the geometry of the CO_2 moiety, which is closer to the geometry of ideal CO_3^{2-}: The O_s−C distance is shorter by 0.09 Å, and the O═C═O bond angle is reduced by 3.5° compared with monodentate formed on terrace sites; see Figures 4 and 6. The calculated DFT adsorption energy is −154 kJ/mol, which is in good agreement with reported experimental values, about −140 kJ/mol at low CO_2 coverage.[37] The calculated wavenumbers (1703, 1327, and 1011 cm^{-1}) resemble the observed wavenumbers at low CO_2 coverage (1670, 1315, and 1000 cm^{-1}) (Figure 10). The difference in wavenumbers ($\Delta\nu_{3h} = 33$, $\Delta\nu_{3l} = 12$, and $\Delta\nu_1 = 11$) follow the trend observed by Jalbout and El-Nahas,[38] who examined harmonic frequencies of formaldehyde-like compounds computed at the B3LYP/6-311++G(3df,3pd) level of theory; high-frequency modes were overestimated and low-frequency modes were somewhat underestimated compared with experimental values. Moreover, this species is also the most thermally stable; it is the only one present after evacuation at 400 °C (Figure 10; the peaks are slightly blue shifted), consistent with the DFT energies for adsorbed CO_2 on MgO (Table 1). Given the agreement between the theoretical and experimental results, the bands at 1670, 1315, 1000, and 850 cm^{-1} may be assigned to CO_2 in monodentate coordination at edge sites. This result contradicts the common assumption that these bands arise from CO_2 chemisorbing in a bidentate configuration.[14,39]

CaO. The computed adsorption energy, −219 kJ/mol, confirms that CO_2 is strongly chemisorbed at the O_{4C} site. The adsorption is considerably stronger here compared to what is found for the O_{5C} site, in accordance with the tendency seen for MgO. The bond distances are about the same as for CO_2 on MgO at O_{4C}, but the O═C═O angle is reduced further, that is, closer to the bond angles of free carbonate. This may be attributed to the greater polarizability of CaO. In addition to the satisfactory agreement between experimental and calculated adsorption energies, the experimental vibrational bands at 1635, 1290−1302, and 970−980 cm^{-1} (Figure 11) are reproduced surprisingly well by the calculated frequencies: 1664, 1316, and 968 cm^{-1}. Hence, we suggest that the bands at 1635, 1290−1302, and 970−980 cm^{-1} arise from CO_2 adsorbed at O_{4C} sites in a monodentate fashion. This amounts to a reinterpretation of earlier, experimental works,[14,39] in which these bands were assigned to CO_2 adsorbed in a bidentate geometry; in the present work, we do not find a stable bidentate geometry for CO_2 on CaO.

3.3. Adsorption at Three-Coordinated O^{2-}. *MgO*. The corner sites yield a richer chemistry than the edge and terrace sites. For MgO, we have found two distinct adsorption modes: bidentate (Figure 8) and tridentate (Figure 9). The calculated adsorption energies are −115 and −152 kJ/mol, respectively. The latter energy is closer to the experimental value of −140 kJ/mol, but the computed energy difference between the two species is too small to constitute any conclusive evidence in favor of the tridentate structure. Efforts were made to find a stable monodentate, as found for CaO (Figure 7) (see below), but these efforts failed as the optimizations invariably gave a tridentate structure (Figure 9), regardless of starting geometry.

The tridentate model exhibits vibrational bands closely similar to the experimental results for a free carbonate ion ($\nu_3 = 1415$, $\nu_1 = 1063$, and $\nu_2 = 879$ cm^{-1}).[34] Our calculated frequencies for the tridentate model appear at $\nu_3 = 1451$, $\nu_1 = 1084$, and $\nu_2 = 906$ cm^{-1}, where the ν_3 mode is doubly degenerate. The carbonate ion is almost planar, as borne out by the fact that all the O═C═O angles are ∼119°. It is not possible to assign any of the experimentally observed bands to tridentate CO_2 at corner sites, but Yanagisawa et al.[15] observed the appearance of a new band after successive evacuation of CO_2 on MgO at elevated temperatures; at room temperature, they observed two distinct sets of bands at 1659, 1329, and 1024 cm^{-1} and 1626, 1273, and 947 cm^{-1}, i.e., in the same regions as Fukuda and Tanabe[14] (Figure 10), but upon evacuation at temperatures between 473 and 673 K, the latter bands disappeared and a weak band at 1439 cm^{-1} emerged. Finally, after evacuation at 823 K, all bands disappeared. The presence of the band at 1439 cm^{-1} only at higher temperatures indicates that the formation of the species takes place through an activated adsorption process. This is also expected for the formation of the tridentate structure in Figure 9, where the O_{3C} site is highly dislocated from its lattice point. Further, the calculated IR intensities support the presence of only one band, namely, the doubly degenerate ν_3 mode at 1451 cm^{-1}, while the ν_1 and ν_2 modes should be nearly invisible due to minor IR intensities (Table 1). The presence of only one IR-active band at 1451 cm^{-1}/1439 cm^{-1} (obtained theoretically and experimentally, respectively), and the assumption of an activated adsorption process, may point to the formation of the tridentate species at high temperatures. We cannot, however, rule out the possibility that the frequency at 1439 cm^{-1} may arise from formation of bulk carbonate. This possibility has not been further investigated.

In the case of the bidentate adsorption mode, the ν_{3h}, ν_{3l}, and ν_1 modes are all IR active, and they are calculated at 1778, 1243, and 932 cm^{-1}, respectively. It is thus most appropriate to compare these wavenumbers with the experimental values at 1630, 1280, and 950 cm^{-1}, where the $\Delta\nu$ values are $\Delta\nu_{3h} = 148$, $\Delta\nu_{3l} = -37$, and $\Delta\nu_1 = -18$. The two latter frequencies are slightly underestimated, but nevertheless in fairly good agreement with observed values, as opposed to the former frequency which is highly overestimated. The large discrepancies found for the calculated ν_{3h} mode may have several causes: insufficiency of basis set employed, cluster size, or the harmonic approximation. Test calculations were carried out to elucidate these points. Cluster size convergence was addressed by using the reduced cluster shown in Figure 3, where the basis sets described in the computational section were employed. The optimization procedure was the same as described in the computational section. The calculated frequencies were $\nu_{3h} = 1811$, $\nu_{3l} = 1247$, and $\nu_1 = 860$ cm^{-1}. We note that the ν_{3h} is blue shifted even further and the ν_1 mode is considerably red shifted compared to what we observe for the full cluster size. Turning to the issue of basis set convergence and anharmonicity of the ν_{3h} mode, a small MgO−CO_2 cluster was constructed to mimic the bidentate at corner site (see Figure 12). The cluster was treated with 6-311+G(d), cc-pVTZ, aug-cc-pVTZ, and aug-cc-pVQZ. The harmonic and anharmonic vibrational modes were calculated for each of the four basis sets, where the

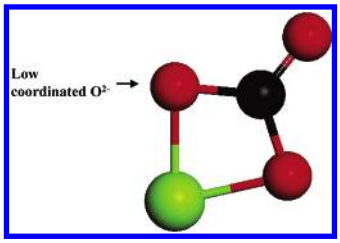

Figure 12. $MgO-CO_2$ cluster employed to test basis set convergence and anharmonicity of the ν_{3h} for bidentate sorption on O_{3c} sites.

anharmonic frequencies were obtained with the anharmonic frequency package implemented in Gaussian 03. Further, the cluster was allowed to fully relax under the geometry optimization. The obtained harmonic frequencies were $\nu_{3h} = 1775$, $\nu_{3h} = 1787$, $\nu_{3h} = 1768$, and $\nu_{3h} = 1771$ cm^{-1} and the anharmonic frequencies were $\nu_{3h} = 1729$, $\nu_{3h} = 1746$, $\nu_{3h} = 1732$, and $\nu_{3h} = 1736$ cm^{-1} for the four above-mentioned basis sets, respectively ($\Delta\nu_{3h} = -46$, $\Delta\nu_{3h} = -41$, $\Delta\nu_{3h} = -36$, $\Delta\nu_{3h} = -35$). Clearly, increasing the basis sets does not influence the vibrational frequency significantly, but the anharmonicity red shifts the ν_{3h} mode, as expected. From the test calculations, we may conclude as follows: Increasing basis set size does not improve the frequency significantly, increased cluster size will probably red shift the ν_{3h} mode, and, finally, an anharmonic correction of the ν_{3h} mode will red shift the mode with about 40−50 cm^{-1} for the 6-311+G(d) basis set. Obviously, the anharmonicity cannot completely account for the blue shift, but assuming a considerable improvement of the ν_{3h} mode by increasing the cluster size may resolve the discrepancy. Under such an assumption, one may assign the bands at 1630, 1280, and 950 cm^{-1} to bidentate CO_2 at a corner site. This is in agreement with previously reported assignments.[14,39]

CaO. As for CO_2 on MgO at corner sites, several different candidates for adsorption modes were found. An energetically favorable monodentate was found (Figure 7), in addition to the bidentate and tridentate depicted in Figures 8 and 9. The two latter species possess bond distances and bond angles very similar to those for CO_2 on MgO. This is also reflected in the calculated frequencies, which are very similar for the two metal oxides (Tables 1 and 2). The artificial split in the ν_{3h} and ν_{3l} modes of the tridentate is due to the combined basis sets employed; the O_{3C} atom is described with 6-31G(d) while the CO_2 has 6-311+G(d). The DFT adsorption energies for the bidentate and tridentate are −182 and −164 kJ/mol, respectively, indicating stable chemisorbed carbonate species. However, the three distinct experimental bands of CO_2 on CaO (Figure 11) are not in the range of the calculated harmonic frequencies at 1778, 1243, and 932 cm^{-1} and 1461, 1423, and 1080 cm^{-1} for the bidentate and tridentate structures, respectively. Therefore, we are led to conclude that these two carbonate species are probably not present in any large concentration at corner sites. This is further borne out by the calculated energy for the monodentate species. It is −222 kJ/mol, demonstrating that this is the most stable adsorption mode at corner sites on CaO. The geometry is quite similar to that of the monodentate species at an edge site, but the O_s-C distance is shortened by 0.03 Å and the C═O bond is elongated by 0.01 Å with respect to the latter. The O═C═O angle is not significantly changed. As mentioned above, this can be attributed to the increased charge flow at corner sites due to the reduced HOMO−LUMO gap. Moreover, the calculated frequency for the symmetric CO stretching (ν_1) is blue shifted 67 cm^{-1} compared with the monodentate edge sites, indicating a stronger O_s-C interaction. The sorption energies are, perhaps unexpectedly, very close; the difference is only 3 kJ/mol in favor of the corner site. This might be explained by electrostatic attraction between two Ca cations adjacent to the adsorption site and the CO_2 oxygen atom; the Ca−O distance is 2.37 Å for monodentate at edge sites and 2.43 Å at corner sites. It thus appears that the electrostatic attraction compensates for the reduced charge transfer seen for O_{4C}. With regard to the frequencies, the theoretical bands at 1603, 1314, and 1035 cm^{-1} reproduce the observed bands that appear after evacuation at 110 °C, namely, 1550−1570, 1308−1315, and 1050 cm^{-1}, very well (see Figure 11); the agreement between the theoretical and experimental results is sufficient to allow us to suggest that the observed bands arise from formation of monodentate CO_2 at corner sites. Again, this is a reinterpretation of earlier, experimental work,[14] in which these bands are assigned to CO_2 adsorbed in a bidentate geometry.

3.4. Unassigned Bands. The adsorption bands arising at higher CO_2 pressure are very similar for MgO and CaO ($\nu_{3h} = 1550$, $\nu_{3l} = 1410$, $\nu_1 = 1050$, $\nu_2 = 860$ cm^{-1} *and* $\nu_{3h} = 1510$, $\nu_{3l} = 1415$, $\nu_1 = 1060$, $\nu_2 = 860$ cm^{-1}, respectively) and most likely represent the same type of carbonate species. The present calculations demonstrate that the ν_1 mode is blue shifted upon shortening the O_s-C distances; see Figures 4−9 and Tables 1 and 2. Reduced O_s-C distances imply a strong O_s-C interaction and significant adsorption energy. Among the calculated ν_1 modes, only the one arising from the tridentate species (Figure 9) is close to 1050 cm^{-1}. The observed values for the ν_1 mode are probably too high to arise from some type of O_s-C interaction, and the ν_1 mode might instead emerge from the C−O stretch in free carbonate. A further indication of free carbonate formation comes from ^{18}O-enriched CO_2 isotopic labeling experiments,[15,16] which prove that scrambling of oxygen takes place to a significant degree on MgO. None of the adsorption modes proposed in the present work are feasible intermediates for an oxygen scrambling mechanism due to their high degree of symmetry, except for the tridentate species in which a tilting of the carbonate might lead to exchange of oxygen. Experimental findings in the literature however indicate that even the tridentate species is not a feasible intermediate for the observed oxygen exchange with MgO: While the IR band assigned to the tridentate species was observed only after heat treatment at temperatures above 473 K,[14] isotopic scrambling was observed by TPD experiments at temperatures as low as 330 K.[16]

A direct oxygen exchange of CO_2 with the metal oxide, without passing through an intermediate, is also not a probable mechanism. We may speculate that the oxygen scrambling proceeds through a free carbonate species formed in conjunction with defective sites at the oxide surface. Corroborating this assumption is the fact that the observed bands are not very different from the vibrational modes of the carbonate ion in the gas phase as measured experimentally.[34] Hence, the bands could arise from some type of slightly perturbed doubly negatively charged carbonate ions at the surface, rather than the monodentate structure suggested in the literature.[39]

4. Implications for Catalysis

An inspiration for this work was to elucidate whether MgO and CaO may play an active role in the dry reforming of alkanes to synthesis gas, either as CO_2 adsorbents or as reaction sites adsorbing CO_2, which may subsequently contribute to the oxidation of carbon-containing species at a neighboring metal site.[12] Physical parameters related to CO_2 adsorption have been calculated based on the theoretical modeling results and are presented in Table 3. The methods and assumption used for the calculations are described below.

TABLE 3: Calculated Free Energy and Equilibrium Constant of Adsorption, Coverage, and Adsorbate Residence Time for Monodentate $CO_{2(ads)}$ at MgO and CaO Sites at 600 °C

ads site (all monodentate)	ΔG (kJ mol^{-1})	K	θ^a	τ (s)
MgO step, O_{4c}	1.7	0.8	0.19	$3\cdot10^{-5}$
CaO step, O_{4c}	−63.3	6121	1.0	0.2
CaO corner, O_{3c}	−66.3	9255	1.0	0.3

[a] Coverages are calculated for $P(CO_2) = 0.3$ atm.

Associative adsorption is always accompanied by entropy loss. The main contribution is loss of translational energy, while frustrated vibrations and rotations represent minor contributions.[40] At 600 °C, a typical propane reforming temperature, the entropy of translation in three dimensions is 178 J/mol K for the CO_2 molecule. The corresponding $T\Delta S$ term amounts to 156 kJ/mol. This number, when combined with the adsorption enthalpies calculated in this work, strongly indicates that only the most favorable adsorption sites are populated at 600 °C. For MgO, this means monodentate CO_2 on steps ($\Delta H_{ads} = -154$ kJ/mol) and (possibly) tridentate CO_2 on corners ($\Delta H_{ads} = -152$ kJ/mol). For CaO, monodentate CO_2 on steps ($\Delta H_{ads} = -219$ kJ/mol) and on corners ($\Delta H_{ads} = -222$ kJ/mol), respectively, are feasible adsorption modes. Free energy values for the monodentate adsorption modes ($\Delta G = \Delta H - T\Delta S$), corresponding equilibrium constants for adsorption ($K = \exp(-\Delta G/RT)$), and the coverage of each site (using a simple Langmuir expression, $\theta = KP_{CO_2}/(1 + KP_{CO_2})$ and assuming a CO_2 partial pressure of 0.3 atm), all at 600 °C, are shown in Table 3. The residence time of the adsorbate, τ, has been calculated by using the vibrational frequency, ν_1, of the O_s-C stretch along the reaction axis as frequency factor and assuming that the activation energy of desorption equals the inverse adsorption enthalpy ($\tau = 1/k = (2\nu_1 c)^{-1} \exp(-\Delta H/RT)$). This assumption implies that the adsorption process is nonactivated, which is reasonable in the case of associative CO_2 adsorption.

The results in Table 3 indicate that the step and corner sites of CaO will be completely covered by CO_2, while the step sites of MgO will be only partly covered (<20%) by CO_2, at 600 °C and 0.3 atm CO_2 partial pressure. Calculations over an extended pressure range (not shown) suggest that the step and corner sites of CaO will be 85% covered already at 1 mbar CO_2 pressure.

The calculated residence time of the CO_2 adsorbate on MgO steps is shorter, while on CaO steps and corners it is longer, than the inverse turnover frequencies reported in the literature for alkane dry reforming over various supported metal catalysts at 600 °C, i.e., typically 0.01−0.10 s. [13,41−44]

5. Conclusions

Quantum chemical investigations of CO_2 adsorption on MgO and CaO have been performed and compared with infrared spectroscopy data from the literature.

Comparison of theoretical and experimental vibrational frequencies allows us to reinterpret earlier experimental results for both MgO and CaO in terms of adsorption of CO_2 on corner and edge sites, respectively. On MgO, CO_2 adsorbs as monodentate on edge sites and bidentate on corner sites. In the case of CaO, CO_2 adsorbs as monodentate on both edge and corner sites.

For both oxides, a third experimentally observed surface species could not be assigned to any of the proposed adsorption modes. Assumption of the existence of mainly unperturbed carbonate ions on the surface is not contradicted by the experimental IR frequencies.

As expected, the calculations suggest that CO_2 adsorbs more strongly on CaO than on MgO. Further, the DFT adsorption energies show that CO_2 interacts more strongly with oxygen sites of low coordination. This is in agreement with the reduction in the Madelung potential for lower coordinated oxygen, as charge flow from surface oxygen to CO_2 may occur at a lower energy cost. On the edge sites, the calculated adsorption energies are ∼65 kJ/mol lower for CaO than for MgO; the corresponding number for corner sites is ∼110 kJ/mol. On the terrace site, no energetically stable CO_2 adsorption mode was found for MgO, as opposed to CaO where the most stable adsorption mode was calculated to be −100 kJ/mol. In any case, none of the adsorption modes on terrace sites possessed calculated frequencies in agreement with the experimental IR-spectra.

Acknowledgment. The Ph.D. grant of M.B.J. is financed by the Norwegian Research Council, under the KOSK program. Thanks are due to the Norwegian Research Council for a grant of computer time through the NOTUR project (account NN2923K).

References and Notes

(1) Xie, S.; Rosynek, M. P.; Lunsford, J. H. *J. Catal*. **1999**, *188*, 32−39.
(2) Lunsford, J. H.; Qiu, P.; Rosynek, M. P.; Yu, Z. *J. Phys. Chem. B* **1998**, *102*, 167−173.
(3) Lin, C. H.; Ito, T.; Wang, J.; Lunsford, J. H. *J. Am. Chem. Soc.* **1987**, *109*, 4808−4810.
(4) Szmigiel, D.; Rarog-Pilecka, W.; Miskiewicz, E.; Glinski, M.; Kielak, M.; Kaszkur, Z.; Kowalczyk, Z. *Appl. Catal., A* **2004**, *273*, 105−112.
(5) Guzman, J.; Gates, B. C.; Bruce C. *J. Catal*. **2004**, *226*, 111−119.
(6) Aytam, H. P.; Akula, V.; Janmanchi, K.; Rama Rao, K. S.;. Rao, P. K.; Gurram, K.; Niemantsverdriet, J. W. *J. Phys. Chem. B* **2002**, *106*, 1024−1031.
(7) Kagawa, K.; Mogi, K.; Tanaka, T. JP 2003019435 A2, 2003.
(8) Yong, Z.; Mata, V. G.; Rodrigues, A. E. *Adsorption* **2001**, *7*, *41*−*50*.
(9) Ding, Y.; Alpay, E. *Chem. Eng. Sci*. **2000**, *55*, 3461−3474.
(10) Ding, Y.; Alpay, E. *Chem. Eng. Sci*. **2000**, *55*, 3929−3940.
(11) Hufton, J. R.; Mayorga, S. *S. Sircar Sep.* **1999**, *45*, 248−256.
(12) Tomishige, K.; Fujimoto, K. *Catal. Surv. Jpn.* **1998**, *2*, 3−15.
(13) Wei, J.; Iglesia, E. *J. Catal*. **2004**, *224*, 370−383.
(14) Fakuda, Y.; Tanabe, K. *Bull. Chem. Soc. Jpn*. **1973**, *46*, 1616−1619.
(15) Yanagisawa, Y.; Takaoka, K.; Yamabe, S. *T. Ito J. Phys. Chem*. **1995**, *99*, 3704−3710.
(16) Yanagisawa, Y.; Takaoka, K.; Yamabe, S., *J. Chem. Soc., Faraday Trans.* **1994**, *90*, 2561−2566.
(17) Shen, J.; Kobe, J. M.; Chen, Y.; Dumesic, J. A. *Langmuir* **1994**, *10*, 3902−3908.
(18) Carrier, X.; Doyle, C. S.; Kendelewicz, T.; Brown, G. E. *Surf. Rev. Lett. 1***999**, *6*, 1237−1245.
(19) Pacchioni, G. *Surf. Sci.* **1993**, *281*, 207−219.
(20) Pacchioni, G.; Ricart, J. M.; Illas, F. *J. Am. Chem. Soc.* **1994**, *116*, 10152−10158.
(21) Nygren, M.; Pettersson, L. G. M. *Chem. Phys. Lett.* **1994**, *230*, 456−462.
(22) Karlsen, E.;. Nygren, M. A.; Pettersson, L. G. M. *J. Phys. Chem. B* **2003**, *107*, 7795−7802.
(23) Snis, A.; Miettinen, H. *J. Phys. Chem. B* **1998**, *102*, 2555−2561.
(24) Karlsen, E. J.; Nygren, M. A.; Pettersson, L. G. M. *J. Phys. Chem. A* **2002**, *106*, 7868−7875.
(25) Di Valentin, C.; Figini, A.; Pacchioni, G., *Surf. Sci.* **2004**, *556*, 145−158.
(26) Bawa, F.; Panas, I. *Phys. Chem. Chem. Phys*. **2001**, *3*, 3042−3047.
(27) Pelmenschikov, A. G.; Morosi, G.; Gamba, A.; Coluccia, S. *J. Phys. Chem*. **1995**, *99*, 15018−22.
(28) Pelmenschikov, A. G.; Morosi, G.; Gamba, A.; Coluccia, S.; Martra, G.; Paukshtis, E. A. *J. Phys. Chem*. **1996**, *100*, 5011−16.
(29) Pelmenschikov, A. G.; Morosi, G.; Gamba, A.; Coluccia, S.; Martra, G.; Pettersson, L. G. M. *J. Phys. Chem. B* **2000**, *104*, 11497−11500.
(30) Pelmenschikov, A. G.; Morosi, G.; Gamba, A, Coluccia, S. *J. Phys. Chem. B* **1998**, *102*, 2226−2231.
(31) Nygren, M. A.; Petterson, L. G. M.; Barandiaran, Z.; Seijo, S. *J. Phys. Chem*. **1992**, *100*, 2010−2018.

(32) Frisch, M. J.; Trucks, G. W.; Schlegel, H. B.; Scuseria, M. A.; Robb, M. A.; Cheeseman, J. R.; Montgomery, J. A.; Vreven, T.; Kudin, K. N.; Burant, J. C.; Miliam, S.; Millam, J. M.; Iyengar, S. S.; Tomasi, J.; Barone, V.; Mennucci, B.; Cossi, M.; Scalmani, G.; Rega, N.; Petterson, G. A.; Nakatsuji, H.; Hada, M.; Ehara, M.; Toyota, K.; Fukada, R.; Hasegawa, J.; Ishida, M.; Nakajima, T.; Honda, Y.; Kitao, O.; Nakai, H.; Klene, M.; Li, X.; Knox, E.; Hratchian, H. P.; Cross, J. B.; Adamo, C.; Jaramillo, J.; Gomperts, R.; Stratmann, R. E.; Yazyev, O.; Austin, A. J.; Cammi, R.; Pomelli, C.; Ochterski, J. W.; Ayala, P. Y.; Morokuma, K.; Voth, G. A.; Salvador, P.; Dannenberg, J. J.; Zakrzewski, V. G.; Dapprich, S.; Daniels, A. D.; Strain, M. C.; Farkas, O.; Malick, D. K.; Rabuck, A. D.; Ragahavachari, K.; Foresman, J. B.; Ortiz, J. V.; Cui, Q.; Baboul, A. G.; Clifford, S.; Cioslowski, J.; Stefanov, B. B.; Liu, G.; Liashenko, A.; Piskorz, P.; Komaromi, I.; Martin, R. L.; Fox, D. J.; Keith, T.; Al-Laham, M. A.; Peng, C. Y.; Nanayakkara, A.; Challacombe, M.; Gill, P. M. W.; Johnson, B.; Chen, W.; Wong, M. W.; Gonzalez, C.; Pople, J. A. *Gassian03* (revision B.04); Gaussian, Inc.: Pittsburgh, PA, 2003.

(33) Simon, S.; Duran, M.; Dannenberg, J. J. *J. Chem. Phys.* **1996**, *105*, 11024−11031.

(34) Herzberg, G. *Infrared and Raman spectra of Polyatomic Molecules*; Van Nostrand: New York, 1945; p 178.

(35) Giamello, E.; Ugliengo, P.; Garrone E. *J. Chem, Soc., Faraday Trans. 1: Phys. Chem. Condens. Phases* **1989**, *85*, 1373−1382.

(36) Beruto, D.; Botter, R.; Searcy, A. W. *J. Phys. Chem.* **1984**, *88*, 4052−4055.

(37) Tichit, D.; Lhouty, M. H.; Guida, A.; Chiche, B. H.; Figueras, F.; Auroux, A.; Baratalini D.; Garrone, E. *J. Catal.* **1995**, *151*, 50−59.

(38) Jalbout A. F.; El-Nahas, A. M. *J. Mol. Struct.* **2004**, *671*, 125−132.

(39) Busca, G.; Lorenzelli, V. *Mater. Chem.* **1982**, *7*, 89−126.

(40) Atkins, P. W. *Physical Chemistry*, 6th ed.; Oxford University Press: Oxford, U.K., 1998; p 586.

(41) Wei, J.; Iglesia, E. *Angew Chem. Int. Ed.* **2004**, *43*, 3685−2688.

(42) Wei, J.; Iglesia, E. *J. Catal.* **2004**, *225*, 116−127.

(43) Wei, J.; Iglesia, E. *J. Phys. Chem. B* **2004**, *108*, 7253−7262.

(44) Olafsen, A.; Slagtern, Å.; Dahl, I. M.; Olsbye, U.; Schuurman, Y.; Mirodatos, C. *J. Catal.* **2005**, *229*, 163−175.